The effects of teleconnections on carbon fluxes of global terrestrial ecosystems

Zaichun Zhu, Shilong Piao, Yaoya Xu, Ana Bastos, Philippe Ciais, Shushi Peng

AGU PUBLICATIONS

Geophysical Research Letters

RESEARCH LETTER
10.1002/2016GL071743

Key Points:
- Seasonal GPP variations of more than 82.1% of the global vegetated lands are significantly affected by major teleconnections
- Teleconnections affect global carbon fluxes through synergistically modulating global temperature and regional precipitation and radiation
- The ENSO, PDO, and AMO strongly control global carbon fluxes, while the Northern Hemisphere teleconnections have only a regional influence

Supporting Information:
- Supporting Information S1

Correspondence to:
S. Piao,
slpiao@pku.edu.cn

Citation:
Zhu, Z., S. Piao, Y. Xu, A. Bastos, P. Ciais, and S. Peng (2017), The effects of teleconnections on carbon fluxes of global terrestrial ecosystems, *Geophys. Res. Lett.*, *44*, 3209–3218, doi:10.1002/2016GL071743.

Received 29 OCT 2016
Accepted 29 MAR 2017
Accepted article online 30 MAR 2017
Published online 14 APR 2017

The effects of teleconnections on carbon fluxes of global terrestrial ecosystems

Zaichun Zhu[1], Shilong Piao[1,2,3], Yaoya Xu[1], Ana Bastos[4], Philippe Ciais[4], and Shushi Peng[1]

[1]Sino-French Institute for Earth System Science, College of Urban and Environmental Sciences, Peking University, Beijing, China, [2]Key Laboratory of Alpine Ecology and Biodiversity, Institute of Tibetan Plateau Research, Chinese Academy of Sciences, Beijing, China, [3]CAS Center for Excellence in Tibetan Plateau Earth Sciences, Chinese Academy of Sciences, Beijing, China, [4]Laboratoire des Sciences du Climat et de l'Environnement, LSCE/IPSL, CEA-CNRS-UVSQ, Universite Paris-Saclay, Gif-sur-Yvette, France

Abstract Large-scale atmospheric circulation patterns (i.e., teleconnections) influence global climate variability patterns and can be studied to provide a simple framework for relating the complex response of ecosystems to climate. This study analyzes the effects of 15 major teleconnections on terrestrial ecosystem carbon fluxes during 1951–2012 using an ensemble of nine dynamic global vegetation models. We map the global pattern of the dominant teleconnections and find that these teleconnections significantly affect gross primary productivity variations over more than 82.1% of the global vegetated area, through mediating the global temperature and regional precipitation and cloud cover. The El Niño–Southern Oscillation, the Pacific Decadal Oscillation, and the Atlantic Multidecadal Oscillation are strongly correlated with global, hemispherical, and continental carbon fluxes and climatic variables, while the Northern Hemisphere teleconnections have only regional influences. Further research regarding the interactions among the teleconnections and the nonstationarity of the relationship between teleconnections and carbon fluxes is needed.

1. Introduction

Carbon fluxes of terrestrial ecosystems are sensitive to the variability of climate. Changes in air temperature affect photosynthetic rates, likely with strong acclimation processes and the length of growing seasons in all regions where temperature drops below 0 during a fraction of the year [*Cong et al.*, 2013; *Liu et al.*, 2016]. Water availability is a rather ubiquitous control of the spatial distribution of gross primary productivity (GPP) [*Beer et al.*, 2010], so that its variations cause significant GPP shifts, in particular in arid regions [*Brienen et al.*, 2015; *Donohue et al.*, 2013; *Poulter et al.*, 2014; *Xu et al.*, 2013; *Zhou et al.*, 2014]. Further, critical water deficits cause soil water potential to drop, causing cavitation and plant mortality. Changes in precipitation have more complex effects because precipitation relates to soil water availability in a nontrivial manner and covary with radiation changes through cloudiness, thus resulting in changes in vegetation productivity, respiration rates, and fire regimes [*Giglio et al.*, 2013; *Xu et al.*, 2011]. The effect of these different climate variables thus cannot be considered individually, even if some variables play a dominant role in a specific ecosystem [*Medlyn et al.*, 2015; *Parmesan and Hanley*, 2015].

Large-scale atmosphere or coupled atmosphere-ocean modes of climate variability, usually referred to as teleconnections (TCs) due to their long-distance range of influence, provide a useful framework to relate carbon fluxes to climate fluctuations, as they incorporate covariability patterns between multiple climate variables at different time scales [*Hallett et al.*, 2004]. Usually, simple indices summarize these modes of climate variability [*Stenseth et al.*, 2003], and attempts have been made to explain changes in structure and functioning of terrestrial ecosystems using them [*Bastos et al.*, 2016; *Gouveia et al.*, 2008; *Potter et al.*, 2004]. Teleconnection indices were used to explain or predict phenology in the northern high latitudes [*Cook et al.*, 2005], changes in vegetation greenness observed from space [*Buermann et al.*, 2003; *Gong and Ho*, 2003], crop yields [*Gonsamo et al.*, 2016; *Iizumi et al.*, 2014], and terrestrial carbon fluxes [*Bastos et al.*, 2013; *Bastos et al.*, 2016; *Potter et al.*, 2003]. Although numerous studies have studied the relationship between El Niño–Southern Oscillation (ENSO), the most prominent global mode of climate variability, and terrestrial carbon fluxes, less attention has been given to other relevant large-scale modes such as Atlantic Multidecadal Oscillation (AMO), Pacific Decadal Oscillation (PDO), Southern Angular Mode (SAM), and the Northern Hemisphere TCs [*Barnston and Livezey*, 1987; *Buermann et al.*, 2003; *Stenseth et al.*, 2003].

With the development of flux tower measurements and satellite techniques, a better knowledge on global terrestrial ecosystem carbon fluxes has been progressively acquired. However, the uncertainties of current data-driven carbon flux products remain significant in the case of respiration. Dynamic global vegetation models (DGVMs), which encapsulate mechanistic understanding of biophysical and biogeochemical ecosystems processes, produce time-varying maps of terrestrial carbon fluxes [*Krinner et al*., 2005; *Piao et al*., 2013; *Sitch et al*., 2003] and can also be used, in particular, with multimodel ensembles which minimize reliance on a single model [*Intergovernmental Panel on Climate Change*, 2013; *Martre et al*., 2015; *Piao et al*., 2015]. Most importantly, DGVMs can provide simulations of long-term vegetation dynamics over large regions, which is valuable for investigating the responses of vegetation to large-scale climate modes. Other methods are unlikely to provide such long-term consistent spatiotemporal information for large-scale vegetation monitoring. For example, flux tower measurements are only available since recent decades [*Forkel et al*., 2016; *Jung et al*., 2010], while satellite observations generally start from the early 1980s [*Tucker et al*., 2005; *Zhu et al*., 2013].

This study aims to provide a systematic picture of the effects of TCs on terrestrial ecosystem carbon fluxes and their underlying mechanisms. To do so, we first analyzed the relationship between gross primary productivity (GPP) estimated from an ensemble of nine DGVMs from the TRENDYv2 project and 15 teleconnection indices to identify in each region if one or several TCs can explain most of the GPP temporal variability, i.e., if there are dominant TCs. Then we gain insights into the underlying mechanisms explaining the impact of dominant TCs and GPP by analyzing its relationship with air temperature, precipitation, and cloud cover. Lastly, we also analyzed the relationship between all 15 TCs, ecosystem carbon fluxes, and climatic variables at global, hemispherical, and subcontinental scales.

2. Material and Methods

2.1. Teleconnection Indices

The existence of quasi-simultaneous physical variations in climate over distant parts of the globe results from the transient behavior of the atmospheric planetary-scale waves that propagate atmospheric anomalies across large extents. Due to their long-distance action, spatially coherent modes climate variations are commonly referred to as teleconnections [*Barnston and Livezey*, 1987; *Wallace et al*., 1992]. The term teleconnection may refer to patterns arising from the internal variability of the atmosphere only also from the coupling between the air and the ocean. In this study, we analyze the TCs that dominate climate variability in the Northern Hemisphere, the Arctic Oscillation (AO), the North Atlantic Oscillation (NAO), the East Atlantic (EA), the East Atlantic/Western Russia (EAWR), the Scandinavia (SCAND), the Polar/Eurasia (polarEA), the West/Pacific (WP), the East Pacific-North Pacific (EPNP), the Pacific/North America (PNA), the Tropical/Northern Hemisphere (TNH), and the Pacific Transition (PT); in the Southern Hemisphere, the Southern Angular Mode (SAM); and three important atmosphere-ocean coupled variability patterns that influence global climate, the El Niño–Southern Oscillation (ENSO), the Pacific Decadal Oscillation (PDO), and the Atlantic Multidecadal Oscillation (AMO).

The 11 first indices refer to Northern Hemisphere atmospheric circulation patterns and are provided by the Climate Prediction Center of the National Oceanic and Atmospheric Administration. These 11 indices were calculated for a northern region between 20°N and 90°N using a rotated principal component analysis (RPCA) of 1000 mbar or 500 mbar geopotential height anomaly monthly fields, as described in *Barnston and Livezey* [1987]. It should be noted that the TNH and PT modes are only expressed during winter and summer, respectively, and thus were excluded from the following analysis. The SAM index was defined as the difference in normalized monthly zonal mean sea level pressure between 40°S and 70°S [*Nan and Li*, 2003]. ENSO is the most important coupled ocean-atmosphere phenomenon driving climate variability. Here we adopted the monthly Multivariate ENSO Index (MEI), which takes into consideration variability both in the atmosphere and in the ocean [*Wolter and Timlin*, 2011]. The PDO and AMO modes are defined as the leading sea surface temperature variability modes in the North Pacific and North Atlantic Ocean, respectively [*Bond and Harrison*, 2000; *Enfield et al*., 2001].

2.2. Dynamic Global Vegetation Models

Global monthly gross primary productivity (GPP), autotrophic respiration (Ra), heterotrophic respiration (Rh), and net biome productivity (NBP) for the period 1951 to 2012 simulated by nine DGVMs (CLM4.5, ISAM, JULES, LPJ, LPX, OCN, ORCHIDEE, VEGAS, and VISIT) were used in this analysis. These models were

coordinated by the project "Trends and drivers of the regional scale sources and sinks of carbon dioxide—version 2" (TRENDYv2), which have been widely used in the research regarding terrestrial ecosystem carbon fluxes [*Le Quéré et al*., 2013; *Schimel et al*., 2015; *Sitch et al*., 2015]. Those ecosystem models were forced with historical changes in atmospheric CO_2 concentration [*Keeling et al*., 2009] and climate fields from the CRU-NCEP data set, nitrogen deposition (in CLM4.5, LPX and OCN), and variable agricultural land cover change from the HYDE data set [*Hurtt et al*., 2011].

2.3. Climate Data

All monthly climate data used for this study were extracted from the CRU-TS (version 3.23) data collection [*Harris et al*., 2014]. We used three climate variables: mean temperature, precipitation, and cloud cover (as a proxy for radiation conditions). The CRU climate data set was selected for monthly time series spanning from 1951 to 2012 at 1° spatial resolution.

Monthly carbon fluxes (GPP, Ra, Rh, and NBP) from DGVMs and climate data (temperature, precipitation, and cloud cover) were first deseasonalized (mean seasonal cycle removed) on a pixel basis to compute monthly anomalies. To eliminate the effects of changes in other factors, e.g., atmospheric CO_2 concentration, nitrogen deposition, or land use change, we detrended the seasonal carbon fluxes anomalies by removing their linear trends. Similarly, all monthly teleconnection indices were integrated over 3 months and detrended. Detrending time series of both land carbon fluxes and teleconnection indices before the correlation analyses is an effective way to retain only variability in the time series and therefore eliminate spurious relationships between time series due to common trends [*Xu et al*., 2013; *Zhou et al*., 2001]. It should be noted that we restricted the analyses between the Northern Hemisphere TCs and carbon fluxes in the Northern Hemisphere continents. The correlation relationships between multimodel ensemble mean (MME) carbon fluxes and teleconnections are estimated using the Pearson's correlation coefficient. We test the correlation relationships using the false discovery rate (FDR) procedure at $p < 0.01$ significance level to avoid overstatement of level of confidence in the correlation relationships [*Wilks*, 2016]. The modelled carbon fluxes were lagged 0, 3, and 6 months relative to teleconnection indices to account for the legacy effects of large-scale atmosphere or coupled atmosphere-ocean modes on terrestrial ecosystem. The correlation between carbon fluxes simulated by individual model and teleconnections were also estimated, and the models are considered to be consistent when at least 6 of the 9 (66.7%) ecosystem models agree with the MME results.

3. Results

3.1. Effects of TCs on Gross Primary Production

We first analyze the relationship between global, hemispheric, and subcontinental GPP and the TCs for different time lags to select only TCs presenting significant relationships and passing the model consistency test (Figure 1 and Figure S1). Global GPP variations (Figure 1a) are found to be more strongly related with ENSO ($r = -0.50$) and PDO ($r = -0.42$). For the Northern Hemisphere, only AMO presents a highly significant relationship with GPP ($r = 0.36$) (Figure 1b), while in the Southern Hemisphere, ENSO and PDO were highly significantly correlated with GPP ($r = -0.54$ and $r = -0.38$, respectively). We subdivide the global vegetated area into 11 subregions according to the definition of the Transcom v3: North American boreal, North American temperate, Europe, Eurasian boreal, Eurasian temperate, South American tropical, South American temperate, Northern Africa, Southern Africa, Tropical Asia, and Australia [*Baker et al*., 2006]. We found that GPP in 7 of the 11 subregions were significantly correlated with ENSO, with absolute correlation coefficients ranging from 0.25 in South American temperate to 0.54 in South American tropical. In the boreal subregions (i.e., North American boreal, Europe, and Eurasian boreal), AMO, EPNP, WP, and PDO were more strongly related to GPP variations than ENSO. The relationships between GPP estimated by multimodel ensemble mean method and TCs are generally consistent with that of the individual models (Figure S2).

For each grid cell, we calculated the correlation between seasonal GPP anomalies and each teleconnection index with zero to two seasonal time lags (equivalent to 0, 3, or 6 months lag of GPP after TCs). Figure S3 shows the spatial pattern of the maximum absolute value of correlation coefficients across all teleconnection index and different time lags. Figure S3 indicates that in some regions, GPP is strongly influenced by more than one teleconnection. For example, GPP in Scandinavia correlates with PDO, AMO, EPNP, WP, AO, SCAN, EA, and EAWR. The AO, NAO, EPNP, WP, and EAWR TCs present regionally heterogeneous correlation patterns with GPP, consisting of negative correlations in some regions and positive in others. On the contrary, the

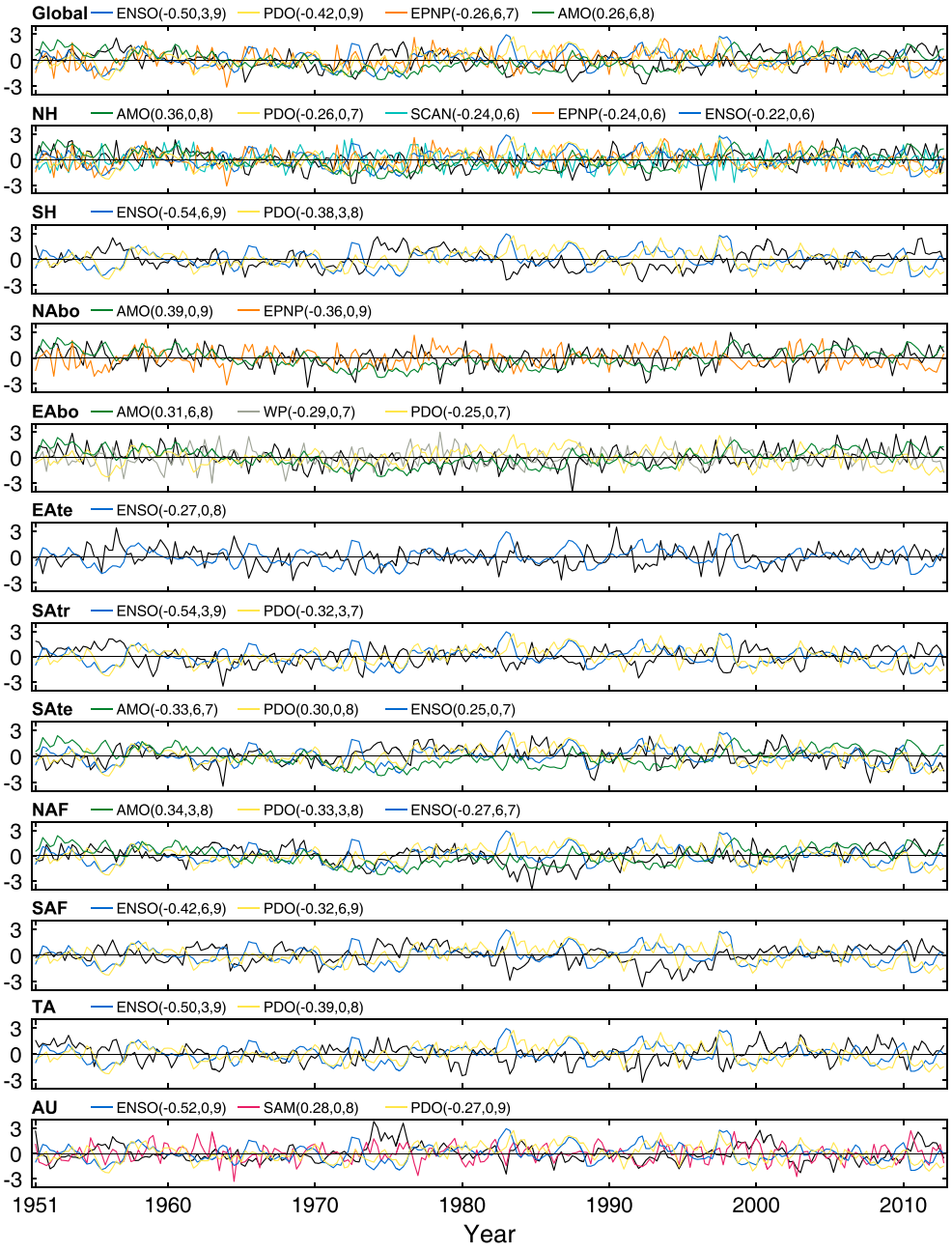

Figure 1. Time series of standardized anomalies in deseasonalized and detrended multimodel ensemble mean (MME) GPP for global, Northern Hemisphere, Southern Hemisphere, and the Transcom v3 regions and their corresponding statistically significantly correlated (false discovery rate procedure at $p = 0.01$ significance test; see section 2) detrended teleconnection indices. Only those correlation relationships pass the model consistency tests (see section 2) are plotted. The numbers in the brackets following teleconnection names show corresponding Pearson's correlation coefficients, lag time, and number of models that agree with the MME results.

majority of pixels related with SCAND present a spatially coherent negative relationship, explaining why SCAND presents a significant relationship with northern hemispheric GPP variations (Figure 1). Figure S4 shows the spatial patterns of the corresponding time lag. The fraction of pixels where significant correlations (FDR ($p < 0.01$)) are found for each teleconnection are presented in Figure S5.

The teleconnection index presenting the maximum absolute value of correlation coefficient with GPP at a given lag of a grid cell was defined as the dominant teleconnection of the pixel, and the corresponding lag step was defined as the optimal lag of this dominant teleconnection. The spatial distribution of the

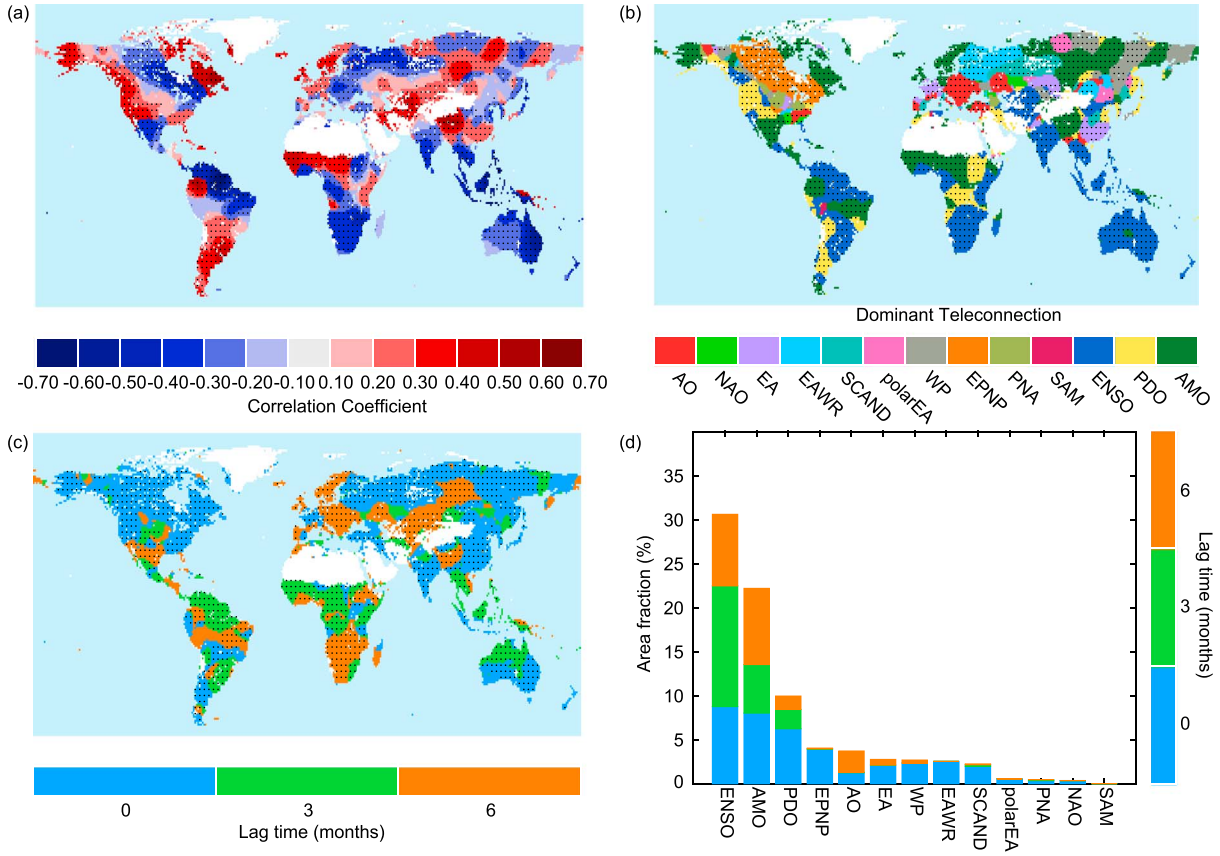

Figure 2. Teleconnection showing the largest correlation with local GPP variations for the period 1951–2012. (a) Spatial pattern of maximum correlation coefficients between ensemble averaging GPP and teleconnection indices. (b) Spatial pattern of teleconnections that can best represent GPP variations. (c) Spatial pattern of lag time of teleconnections in Figure 2b. (d) Statistics of fraction of global vegetated area dominated by each teleconnection and its corresponding time lags. The regions labeled by black dots means that at least six models agree with the multimodel mean outputs.

correlation coefficients between the dominant TC and GPP at the pixel level and the corresponding teleconnection are shown in Figures 2a and 2b. More than 82.1% of the global vegetated area presents significant and consistent GPP correlations (FDR ($p < 0.01$)). Consistent with Figure 1, ENSO is the dominant teleconnection associated with variations of GPP in tropical and temperate regions, correlating significantly with GPP in 61.7% of the global vegetated area (Figure S5) and being the dominant mode over 30.6% of the area. In the Northern Hemisphere, the spatial pattern of dominant TC is more heterogeneous, with the spatial pattern of the dominant TC having only a limited regional extent related to their influence on climate conditions. For example, GPP variations in Eastern Europe are dominantly associated with AO, NAO, and EA, in accordance with the predominance of these modes in the atmospheric circulation of this region [*Cho et al.*, 2014; *Gouveia et al.*, 2008; *Trigo et al.*, 2008]. Similarly, the EPNP that mainly impacts the middle to high latitudes of North America also dominated the GPP variations in this region [*Bell and Janowiak*, 1995].

Our analysis also indicates noticeable lag effects of TCs on variations of GPP (Figure 2c). The fractions of the global vegetated area where variations of GPP were dominated by a certain teleconnection with 0, 3, and 6 month lags are 38.4%, 21.8%, and 21.9%, respectively. The spatial distribution of the lag time is fragmented, although GPP variations in the Northern Hemisphere appear to be mostly dominated by zero lag correlations, irrespective of the teleconnection considered (Figure 2c). Large lagged effects are observed in parts of Africa and North America, generally associated with ENSO and consistent with the different timings of ENSO-induced climate impacts in these regions, e.g., for precipitation in Western Australia and southwest South America [*Diaz et al.*, 2001]. Figure 2d shows the area fraction of each dominant teleconnection that is most significantly correlated with GPP.

Previous studies investigated the effects of TCs on terrestrial ecosystems fluxes using a limited set of common teleconnection indices. Some of them found little spatial correlation between those teleconnection indices

and terrestrial ecosystem variables across large areas [*Buermann et al*., 2003; *Stenseth et al*., 2003]. One possible reason is that teleconnection indices are inherently simplified indicators of complex space and time variability of atmospheric or oceanic information, and a single indicator is unlikely to represent all climatic variability features over a large area [*Barnston and Livezey*, 1987; *Stenseth et al*., 2003]. This is especially the case in the Northern Hemisphere where each teleconnection explains relatively small fractions of atmospheric variability in a given region and where climate variability is modulated by the coupling of different TCs [*Comas-Bru and McDermott*, 2014]. The heterogeneous pattern of correlation coefficients between GPP and TCs in the Northern Hemisphere suggests that future research about ecosystem variability in this region should focus on the regional effects of TCs rather than trying to link large-scale hemispheric climatic and ecological variability focusing only on one or two teleconnection indices.

3.2. The Mechanisms of TCs in Influencing GPP Variations

Global GPP variations are largely explained by variations in climate conditions [*Beer et al*., 2010; *Piao et al*., 2006]. The correlations found between TCs and GPP must derive from the impact of the TCs on the relevant climate variables that influence GPP. Therefore, we calculated the partial correlation between the dominant teleconnection indices and seasonally integrated climate anomalies (temperature, precipitation, and cloud cover) for the period 1951 to 2012. Our results show that the dominant TCs (Figure 2) in the northern high latitudes, South America tropical, Africa, Eurasia temperate, Tropical Asia, and Australia are strongly linked to temperature variations (Figure 3a). The TCs linked to precipitation are mainly in Europe, Siberia, South Asia, and tropical regions and sporadically in other vegetated areas (Figure 3b). In south South America, Europe, east Australia, and other fragmentary vegetated areas, the dominant TCs are more strongly associated with cloud cover (Figure 3c). Figure 3d shows that in most regions, TCs are correlated with more than one variable, highlighting their role in driving covariability of different climatic drivers of ecosystem activity.

3.3. Effects of TCs on Terrestrial Carbon Fluxes and Climate

To further illustrate the effects of TCs on terrestrial carbon fluxes, we calculated the correlation coefficients between teleconnection indices and climatic variables and carbon fluxes simulated by TRENDY models at global, hemispheric, and subcontinental scales for the period 1951 to 2012 (Figure 4). ENSO, PDO, and AMO dominate global terrestrial sinks, presenting negative correlation. The negative correlation between global NBP and the three climate patterns is explained by different responses of ecosystems. During positive phases of ENSO, warmer and drier conditions over the Southern Hemisphere are associated with decreases in both GPP and respiration, the former being stronger than the latter and leading to lower than average NBP. The PDO is found to have similar impacts as ENSO, as expected from their relatively similar effects on the driving climate variables [*Diaz et al*., 2001]. On the contrary, the negative correlation between AMO and NBP is dominated by the effect of higher temperatures (during positive phases) on autotrophic and heterotrophic respiration in the Southern Hemisphere, as well as in North America.

Relationships between the northern hemispheric TCs and terrestrial carbon fluxes are considerably weaker in all continents (Figure 4). The weak contribution of Northern Hemisphere TCs to variations in the terrestrial CO_2 sink in the DGVMs is largely explained by the fact that a large number of atmospheric circulation patterns have a strong influence in northern carbon fluxes, but each is influencing relatively small regions. As these TCs are mostly independent of each other, their variations lead to partly offsetting effects on the hemispheric and global scale, contrasting with the more synchronous dynamics of ecosystems between the three tropical continents.

However, it should be noted that our predefined seasonal time scale analyses would limit the interpretation of the effects of teleconnections with high-frequency variability (e.g., AO and NAO) on carbon fluxes. Future multi–time scale analyses are necessary to improve our knowledge of such ocean-atmosphere-land mechanisms. It should also be noted that the relationship between TCs and carbon fluxes is not likely to be stationary [*Solberg et al*., 2002]. Although our study analyzed the responses of land carbon fluxes to the major TCs for a relatively long period by taking advantage of DGVMs, it should be kept in mind that it is not guaranteed that our results may be expanded to other time periods. In addition, we should be aware that long-term land carbon fluxes simulated by state-of-the-art DGVMs still have notable uncertainties due to parameterization and structure deficiencies in the ecosystem models, even if the ensemble of nine individual ecosystem models allows characterization of model spread. The development of flux tower measuring carbon fluxes

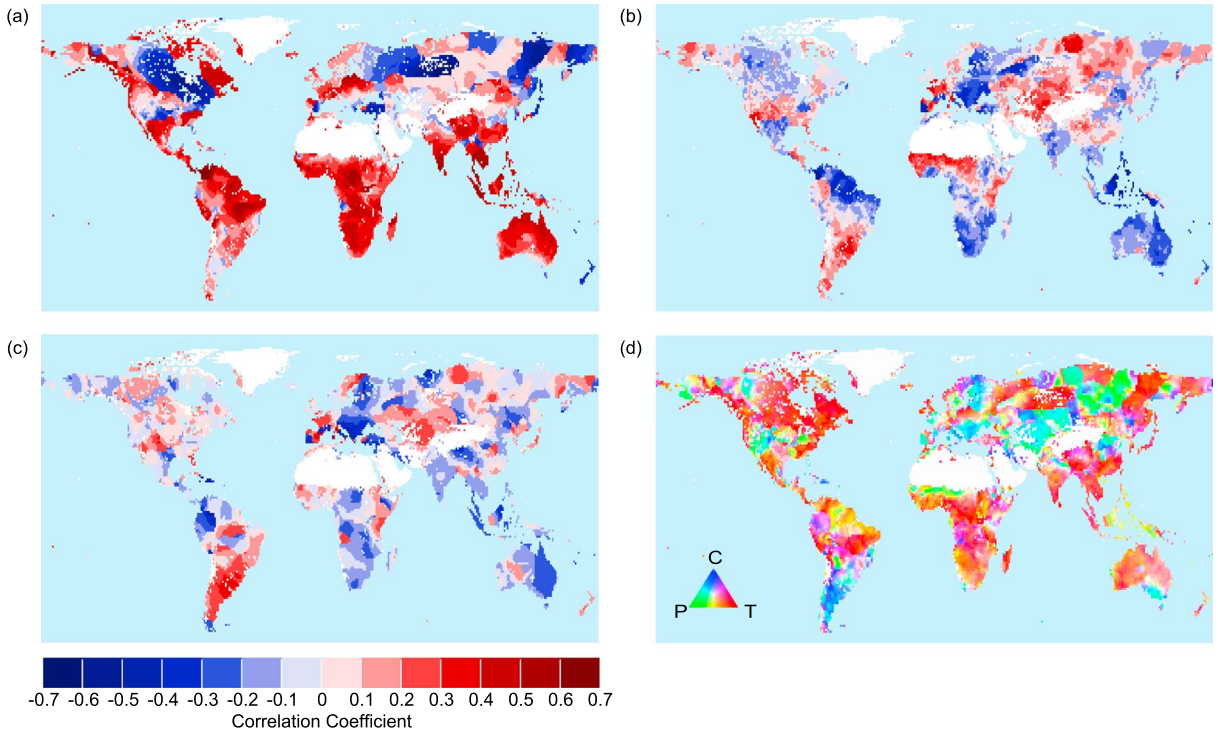

Figure 3. Spatial patterns of correlation coefficients between dominant teleconnection indices and (a) air temperature (*T*), (b) precipitation (*P*), and (c) cloud cover (*C*). (d) Spatial patterns of combinations of correlation between climatic variables and dominant teleconnections.

allows us to bring independent data-driven CO_2 flux estimates to study the relationships between teleconnections and carbon fluxes and compare them with those obtained from ecosystem models [*Desai et al.*, 2016; *Wharton et al.*, 2009]. We thus calculated global and regional correlations between

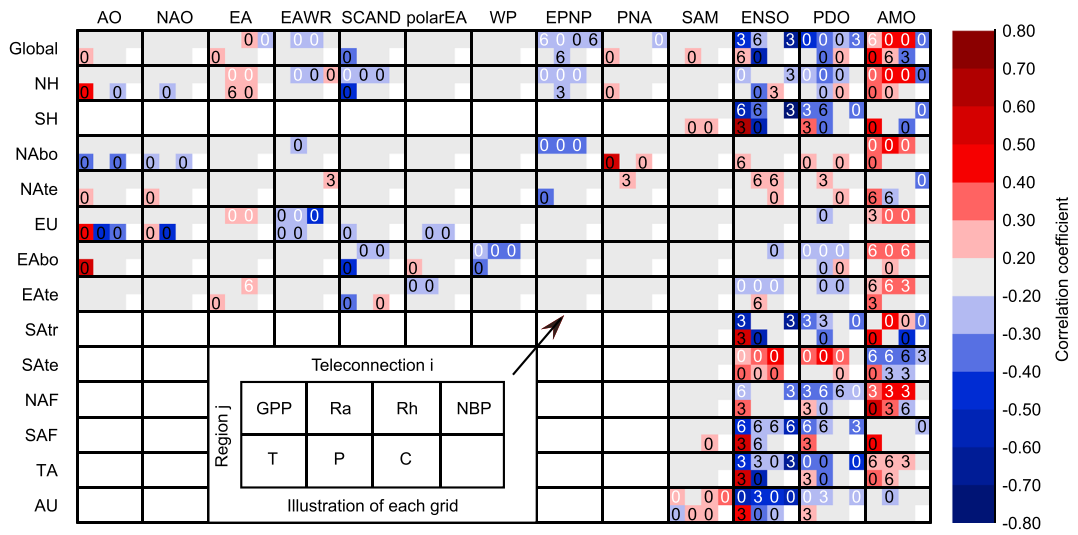

Figure 4. Relationships between teleconnection indices and terrestrial ecosystem carbon fluxes and climatic variables at global, hemispherical, and subregional scales according to the Transcom v3 definition. Each grid labeled by region names and teleconnection names were further divided into two subrows. Color of the first row shows correlation between teleconnection indices and GPP, Ra, Rh, and NBP (grid cells from left to right). Color of the second row shows correlation between teleconnection indices and temperature, precipitation, and cloud cover. The numbers in the subgrids indicate the lag time of carbon fluxes and climatic variables time series behind teleconnections. The lag time numbers of carbon fluxes are shown in white if the correlation relationships pass false discovery rate adjusted significance test and the model consistency test (see section 2).

teleconnections and CO_2 fluxes based on the extrapolation of flux tower measurements using machine-learning algorithms from the FLUXCOM project for the period 1982–2012 [*Jung et al*., 2017] and compared them to that of the TRENDY modelled fluxes. The results indicate that the correlation relationships with FLUXCOM and TRENDY are generally consistent with each other in terms of both correlation coefficient and lag time (Figure S6), which increases the confidence of the TRENDY analyses that cover a longer period (1951–2012).

4. Conclusions

Previous studies have suggested that large-scale atmospheric circulation patterns may provide a framework to simplify the study of the link between climate and ecological variability. However, most of these studies have focused on one single teleconnection, generally ENSO (at the global scale), or NAO (in Eurasia). Our study provides a comprehensive analysis of the effects of TCs on variations of global and regional terrestrial ecosystem carbon fluxes. Our results reveal that ENSO, PDO, and to a lesser extent AMO dominate variability in global, hemispherical, and continental carbon fluxes and climatic variables, while the Northern Hemisphere TCs show more regional influences. Several communities have found it useful to rely on teleconnection indices to evaluate ecological and environmental variability from local to global scales [*Bastos et al*., 2013; *Bastos et al*., 2016; *Cho et al*., 2014; *Hallett et al*., 2004]. The global picture of the spatial distribution of dominant teleconnections described here provides insights on selecting the most suitable teleconnection for local to regional biological studies. For example, our results suggest that AMO is the best teleconnection to analyze seasonal variation of GPP in the Tibetan Plateau and might be a potential driving mechanism of the Sahel regreening [*Dardel et al*., 2014]. We investigated the mechanisms linking the dominant teleconnection and GPP variations through three key climate conditions, i.e., air temperature, precipitation, and radiation (cloud cover as proxy). We find that TCs may be linked to variations in the carbon fluxes through, in general, their control on more than one climate variable. This highlights the potential of these patterns to better represent variability in ecosystem activity since they aggregate the combined variability patterns of temperature, water, and radiation.

With the increasing understanding of Earth system processes and improving ability to predict future teleconnections [*Keenlyside et al*., 2008; *Meehl et al*., 2013], it is likely that our results could be used to guide projection of future carbon flux variations [*Luo et al*., 2015]. However, it should be noted that teleconnection indices generally integrate a pattern of changes for different meteorological variables, which drive variations of terrestrial carbon fluxes. The sensitivities of carbon fluxes to constellations of climate variables can be extremely complex and might vary in space and time [*Piao et al*., 2014; *Wang et al*., 2014]. Furthermore, there is evidence that teleconnection patterns may interact among themselves [*Ruprich-Robert and Cassou*, 2015] and in their impacts [*Bastos et al*., 2016; *Comas-Bru and McDermott*, 2014; *López-Moreno and Vicente-Serrano*, 2008] and be influenced by human activity [*Stevenson*, 2012]. Since many of these patterns present very low frequency variability, long time series are required to properly address these issues. Although Earth observation data sets are still relatively short to evaluate these questions, our results indicate that models are able to capture the relationship between TCs and ecosystems and may be used to further investigate the nonstationary relationship between TCs and terrestrial ecosystem carbon fluxes or the interactions among the TCs and their effects on ecosystem activities.

Acknowledgments
This study was supported by the National Basic Research Program of China (grant 2013CB956303), the National Natural Science Foundation of China (41561134016), and National Youth Top-notch Talent Support Program in China. We thank Pierre Friedlingstein for constructive suggestions on the data and method used in this study. We thank the TRENDY modelling group for providing the TRENDYv2 model data, which are available on reasonable request (contact Stephen Sitch and Pierre Friedlingstein). The teleconnection data are available at the Climate Prediction Center of the National Oceanic and Atmospheric Administration (http://www.cpc.ncep.noaa.gov/); The CRU TS v3.23 climate data are available through the Climatic Research Unit (https://crudata.uea.ac.uk/cru/data/hrg/cru_ts_3.23/).

References

Baker, D. F., et al. (2006), TransCom 3 inversion intercomparison: Impact of transport model errors on the interannual variability of regional CO_2 fluxes, 1988–2003, *Global Biogeochem. Cycles*, *20*, GB1002, doi:10.1029/2004GB002439.

Barnston, A. G., and R. E. Livezey (1987), Classification, seasonality and persistence of low-frequency atmospheric circulation patterns, *Mon. Weather Rev.*, *115*(6), 1083–1126, doi:10.1175/1520-0493(1987)115<1083:CSAPOL>2.0.CO;2.

Bastos, A., S. W. Running, C. Gouveia, and R. M. Trigo (2013), The global NPP dependence on ENSO: La Niña and the extraordinary year of 2011, *J. Geophys. Res. Biogeosci.*, *118*, 1247–1255, doi:10.1002/jgrg.20100.

Bastos, A., et al. (2016), European land CO_2 sink influenced by NAO and East-Atlantic pattern coupling, *Nat. Commun.*, *7*, 10315, doi:10.1038/ncomms10315.

Beer, C., et al. (2010), Terrestrial gross carbon dioxide uptake: Global distribution and covariation with climate, *Science*, *329*(5993), 834–838, doi:10.1126/science.1184984.

Bell, G. D., and J. E. Janowiak (1995), Atmospheric circulation associated with the Midwest floods of 1993, *Bull. Am. Meteorol. Soc.*, *76*(5), 681–695.

Bond, N. A., and D. E. Harrison (2000), The Pacific Decadal Oscillation, air-sea interaction and central North Pacific winter atmospheric regimes, *Geophys. Res. Lett.*, *27*(5), 731–734, doi:10.1029/1999GL010847.

Brienen, R. J. W., et al. (2015), Long-term decline of the Amazon carbon sink, *Nature*, *519*(7543), 344–348, doi:10.1038/nature14283.
Buermann, W., B. Anderson, C. J. Tucker, R. E. Dickinson, W. Lucht, C. S. Potter, and R. B. Myneni (2003), Interannual covariability in Northern Hemisphere air temperatures and greenness associated with El Niño–Southern Oscillation and the Arctic Oscillation, *J. Geophys. Res.*, *108*(D13), 4396, doi:10.1029/2002JD002630.
Cho, M. H., G. H. Lim, and H. J. Song (2014), The effect of the wintertime Arctic Oscillation on springtime vegetation over the northern high latitude region, *Asia-Pac. J. Atmos. Sci.*, *50*(1), 15–21.
Comas-Bru, L., and F. McDermott (2014), Impacts of the EA and SCA patterns on the European twentieth century NAO–winter climate relationship, *Q. J. R. Meteorol. Soc.*, *140*(679), 354–363, doi:10.1002/qj.2158.
Cong, N., T. Wang, H. Nan, Y. Ma, X. Wang, R. B. Myneni, and S. Piao (2013), Changes in satellite-derived spring vegetation green-up date and its linkage to climate in China from 1982 to 2010: A multimethod analysis, *Global Change Biol.*, *19*(3), 881–891, doi:10.1111/gcb.12077.
Cook, B. I., T. M. Smith, and M. E. Mann (2005), The North Atlantic Oscillation and regional phenology prediction over Europe, *Global Change Biol.*, *11*(6), 919–926, doi:10.1111/j.1365-2486.2005.00960.x.
Dardel, C., L. Kergoat, P. Hiernaux, E. Mougin, M. Grippa, and C. J. Tucker (2014), Re-greening Sahel: 30 years of remote sensing data and field observations (Mali, Niger), *Remote Sens. Environ.*, *140*, 350–364, doi:10.1016/j.rse.2013.09.011.
Desai, A. R., G. Wohlfahrt, M. J. Zeeman, G. Katata, W. Eugster, L. Montagnani, D. Gianelle, M. Mauder, and H. P. Schmid (2016), Montane ecosystem productivity responds more to global circulation patterns than climatic trends, *Environ. Res. Lett.*, *11*(2), 024013, doi:10.1088/1748-9326/11/2/024013.
Diaz, H. F., M. P. Hoerling, and J. K. Eischeid (2001), ENSO variability, teleconnections and climate change, *Int. J. Climatol.*, *21*(15), 1845–1862, doi:10.1002/joc.631.
Donohue, R. J., M. L. Roderick, T. R. McVicar, and G. D. Farquhar (2013), Impact of CO_2 fertilization on maximum foliage cover across the globe's warm, arid environments, *Geophys. Res. Lett.*, *40*, 3031–3035, doi:10.1002/grl.50563.
Enfield, D. B., A. M. Mestas-Nuñez, and P. J. Trimble (2001), The Atlantic Multidecadal Oscillation and its relation to rainfall and river flows in the continental U.S, *Geophys. Res. Lett.*, *28*(10), 2077–2080, doi:10.1029/2000GL012745.
Forkel, M., N. Carvalhais, C. Rödenbeck, R. Keeling, M. Heimann, K. Thonicke, S. Zaehle, and M. Reichstein (2016), Enhanced seasonal CO_2 exchange caused by amplified plant productivity in northern ecosystems, *Science*, *351*(6274), 696–699, doi:10.1126/science.aac4971.
Giglio, L., J. T. Randerson, and G. R. van der Werf (2013), Analysis of daily, monthly, and annual burned area using the fourth-generation global fire emissions database (GFED4), *J. Geophys. Res. Biogeosci.*, *118*, 317–328, doi:10.1002/jgrg.20042.
Gong, D. Y., and C. H. Ho (2003), Detection of large-scale climate signals in spring vegetation index (normalized difference vegetation index) over the Northern Hemisphere, *J. Geophys. Res.*, *108*(D16), 4498, doi:10.1029/2002JD002300.
Gonsamo, A., J. M. Chen, and D. Lombardozzi (2016), Global vegetation productivity response to climatic oscillations during the satellite era, *Global Change Biol.*, *22*(10), 3414–3426, doi:10.1111/gcb.13258.
Gouveia, C., R. M. Trigo, C. C. DaCamara, R. Libonati, and J. M. C. Pereira (2008), The North Atlantic Oscillation and European vegetation dynamics, *Int. J. Climatol.*, *28*(14), 1835–1847, doi:10.1002/joc.1682.
Hallett, T. B., T. Coulson, J. G. Pilkington, T. H. Clutton-Brock, J. M. Pemberton, and B. T. Grenfell (2004), Why large-scale climate indices seem to predict ecological processes better than local weather, *Nature*, *430*(6995), 71–75, doi:10.1038/nature02708.
Harris, I., P. D. Jones, T. J. Osborn, and D. H. Lister (2014), Updated high-resolution grids of monthly climatic observations—The CRU TS3.10 dataset, *Int. J. Climatol.*, *34*(3), 623–642, doi:10.1002/joc.3711.
Hurtt, G. C., et al. (2011), Harmonization of land-use scenarios for the period 1500–2100: 600 years of global gridded annual land-use transitions, wood harvest, and resulting secondary lands, *Clim. Change*, *109*(1–2), 117–161, doi:10.1007/s10584-011-0153-2.
Iizumi, T., J.-J. Luo, A. J. Challinor, G. Sakurai, M. Yokozawa, H. Sakuma, M. E. Brown, and T. Yamagata (2014), Impacts of El Niño Southern Oscillation on the global yields of major crops, *Nat. Commun.*, *5*, 3712, doi:10.1038/ncomms4712.
Intergovernmental Panel on Climate Change (2013), Climate change 2013: The physical science basis. Contribution of Working Group I to the Fifth Assessment Report of the Intergovernmental Panel on Climate Change, 1535 pp., Cambridge Univ. Press, Cambridge, U. K., and New York.
Jung, M., et al. (2010), Recent decline in the global land evapotranspiration trend due to limited moisture supply, *Nature*, *467*(7318), 951–954, doi:10.1038/nature09396.
Jung, M., et al. (2017), Compensatory water effects link yearly global land CO_2 sink changes to temperature, *Nature*, *541*(7638), 516–520, doi:10.1038/nature20780.
Keeling, R. F., S. C. Piper, A. F. Bollenbacher, and J. S. Walker (2009), Atmospheric CO_2 records from sites in the SIO air sampling network, in *Trends: A Compendium of Data on Global Change. Carbon Dioxide Information Analysis Center*, Oak Ridge Natl. Lab., U.S. Dep. of Energy, Oak Ridge, Tenn., doi:10.3334/CDIAC/atg.035.
Keenlyside, N. S., M. Latif, J. Jungclaus, L. Kornblueh, and E. Roeckner (2008), Advancing decadal-scale climate prediction in the North Atlantic sector, *Nature*, *453*(7191), 84–88, doi:10.1038/nature06921.
Krinner, G., N. Viovy, N. de Noblet-Ducoudré, J. Ogée, J. Polcher, P. Friedlingstein, P. Ciais, S. Sitch, and I. C. Prentice (2005), A dynamic global vegetation model for studies of the coupled atmosphere-biosphere system, *Global Biogeochem. Cycles*, *19*, GB1015, doi:10.1029/2003GB002199.
Le Quéré, C., et al. (2013), Global carbon budget 2013, *Earth Syst. Sci. Data Discuss.*, *6*(2), 689–760, doi:10.5194/essdd-6-689-2013.
Liu, Q., Y. H. Fu, Z. Zhu, Y. Liu, Z. Liu, M. Huang, I. A. Janssens, and S. Piao (2016), Delayed autumn phenology in the Northern Hemisphere is related to change in both climate and spring phenology, *Global Change Biol.*, *22*(11), 3702–3711, doi:10.1111/gcb.13311.
López-Moreno, J. I., and S. M. Vicente-Serrano (2008), Positive and negative phases of the wintertime North Atlantic Oscillation and drought occurrence over Europe: A multitemporal-scale approach, *J. Clim.*, *21*(6), 1220–1243, doi:10.1175/2007JCLI1739.1.
Luo, Y. Q., T. F. Keenan, and M. Smith (2015), Predictability of the terrestrial carbon cycle, *Global Change Biol.*, *21*(5), 1737–1751, doi:10.1111/gcb.12766.
Martre, P., et al. (2015), Multimodel ensembles of wheat growth: Many models are better than one, *Global Change Biol.*, *21*(2), 911–925, doi:10.1111/gcb.12768.
Medlyn, B. E., et al. (2015), Using ecosystem experiments to improve vegetation models, *Nat. Clim. Change*, *5*(6), 528–534, doi:10.1038/nclimate2621.
Meehl, G. A., et al. (2013), Decadal climate prediction: An update from the trenches, *Bull. Am. Meteorol. Soc.*, *95*(2), 243–267.
Nan, S., and J. Li (2003), The relationship between the summer precipitation in the Yangtze River valley and the boreal spring Southern Hemisphere annular mode, *Geophys. Res. Lett.*, *30*(24), 2266, doi:10.1029/2003GL018381.
Parmesan, C., and M. E. Hanley (2015), Plants and climate change: Complexities and surprises, *Ann. Bot. London*, *116*(6), 849–864.

Piao, S. L., J. Y. Fang, and J. S. He (2006), Variations in vegetation net primary production in the Qinghai-Xizang Plateau, China, from 1982 to 1999, *Clim. Change*, *74*(1–3), 253–267, doi:10.1007/s10584-005-6339-8.

Piao, S. L., et al. (2013), Evaluation of terrestrial carbon cycle models for their response to climate variability and to CO_2 trends, *Global Change Biol.*, *19*(7), 2117–2132, doi:10.1111/gcb.12187.

Piao, S. L., et al. (2014), Evidence for a weakening relationship between interannual temperature variability and northern vegetation activity, *Nat. Commun.*, *5*, 5018, doi:10.1038/ncomms6018.

Piao, S., et al. (2015), Detection and attribution of vegetation greening trend in China over the last 30 years, *Global Change Biol.*, *21*(4), 1601–1609, doi:10.1111/gcb.12795.

Potter, C., S. Klooster, M. Steinbach, P. Tan, V. Kumar, S. Shekhar, R. Nemani, and R. Myneni (2003), Global teleconnections of climate to terrestrial carbon flux, *J. Geophys. Res.*, *108*(D17), 4556, doi:10.1029/2002JD002979.

Potter, C., S. Klooster, M. Steinbach, P.-N. Tan, V. Kumar, S. Shekhar, and C. R. D. Carvalho (2004), Understanding global teleconnections of climate to regional model estimates of Amazon ecosystem carbon fluxes, *Global Change Biol.*, *10*(5), 693–703, doi:10.1111/j.1529-8817.2003.00752.x.

Poulter, B., et al. (2014), Contribution of semi-arid ecosystems to interannual variability of the global carbon cycle, *Nature*, *509*(7502), 600–603, doi:10.1038/nature13376.

Ruprich-Robert, Y., and C. Cassou (2015), Combined influences of seasonal East Atlantic pattern and North Atlantic Oscillation to excite Atlantic multidecadal variability in a climate model, *Clim. Dyn.*, *44*(1), 229–253.

Schimel, D., B. B. Stephens, and J. B. Fisher (2015), Effect of increasing CO_2 on the terrestrial carbon cycle, *Proc. Natl. Acad. Sci.*, *112*(2), 436–441, doi:10.1073/pnas.1407302112.

Sitch, S., et al. (2003), Evaluation of ecosystem dynamics, plant geography and terrestrial carbon cycling in the LPJ dynamic global vegetation model, *Global Change Biol.*, *9*(2), 161–185, doi:10.1046/j.1365-2486.2003.00569.x.

Sitch, S., P. Friedlingstein, N. Gruber, S. Jones, G. Murray-Tortarolo, A. Ahlström, S. C. Doney, H. Graven, C. Heinze, and C. Huntingford (2015), Recent trends and drivers of regional sources and sinks of carbon dioxide, *Biogeosciences*, *12*(3), 653–679, doi:10.5194/bg-12-653-2015.

Solberg, B. Ø., A. Hofgaard, and H. Hytteborn (2002), Shifts in radial growth responses of coastal *Picea abies* induced by climatic change during the 20th century, central Norway, *Ecoscience*, *9*(1), 79–88.

Stenseth, N. C., G. Ottersen, J. W. Hurrell, A. Mysterud, M. Lima, K. S. Chan, N. G. Yoccoz, and B. Adlandsvik (2003), Studying climate effects on ecology through the use of climate indices: The North Atlantic Oscillation, El Niño Southern Oscillation and beyond, *Proc. R. Soc. B Biol. Sci.*, *270*(1529), 2087–2096.

Stevenson, S. L. (2012), Significant changes to ENSO strength and impacts in the twenty-first century: Results from CMIP5, *Geophys. Res. Lett.*, *39*, L17703, doi:10.1029/2012GL052759.

Trigo, R. M., M. A. Valente, I. F. Trigo, P. M. A. Miranda, A. M. Ramos, D. Paredes, and R. García-Herrera (2008), The impact of North Atlantic wind and cyclone trends on European precipitation and significant wave height in the Atlantic, *Ann. N. Y. Acad. Sci.*, *1146*(1), 212–234.

Tucker, C. J., J. E. Pinzon, M. E. Brown, D. A. Slayback, E. W. Pak, R. Mahoney, E. F. Vermote, and N. El Saleous (2005), An extended AVHRR 8-km NDVI dataset compatible with MODIS and SPOT vegetation NDVI data, *Int. J. Remote Sens.*, *26*(20), 4485–4498, doi:10.1080/01431160500168686.

Wallace, J. M., C. Smith, and C. S. Bretherton (1992), Singular value decomposition of wintertime sea-surface temperature and 500-Mb height anomalies, *J. Clim.*, *5*(6), 561–576, doi:10.1175/1520-0442(1992)005<0561:SVDOWS>2.0.CO;2.

Wang, X. H., et al. (2014), A two-fold increase of carbon cycle sensitivity to tropical temperature variations, *Nature*, *506*(7487), 212–215, doi:10.1038/nature12915.

Wharton, S., L. Chasmer, M. Falk, and K. T. Paw U (2009), Strong links between teleconnections and ecosystem exchange found at a Pacific Northwest old-growth forest from flux tower and MODIS EVI data, *Global Change Biol.*, *15*(9), 2187–2205, doi:10.1111/j.1365-2486.2009.01952.x.

Wilks, D. S. (2016), "The stippling shows statistically significant grid points": How research results are routinely overstated and overinterpreted, and what to do about it, *Bull. Am. Meteorol. Soc.*, *97*(12), 2263–2273.

Wolter, K., and M. S. Timlin (2011), El Niño/Southern Oscillation behaviour since 1871 as diagnosed in an extended multivariate ENSO index (MEI.Ext), *Int. J. Climatol.*, *31*(7), 1074–1087, doi:10.1002/joc.2336.

Xu, L. A., A. Samanta, M. H. Costa, S. Ganguly, R. R. Nemani, and R. B. Myneni (2011), Widespread decline in greenness of Amazonian vegetation due to the 2010 drought, *Geophys. Res. Lett.*, *38*, L07402, doi:10.1029/2011GL046824.

Xu, L., et al. (2013), Temperature and vegetation seasonality diminishment over northern lands, *Nat. Clim. Change*, *3*(6), 581–586.

Zhou, L. M., C. J. Tucker, R. K. Kaufmann, D. Slayback, N. V. Shabanov, and R. B. Myneni (2001), Variations in northern vegetation activity inferred from satellite data of vegetation index during 1981 to 1999, *J. Geophys. Res.*, *106*(D17), 20,069–20,083, doi:10.1029/2000JD000115.

Zhou, L. M., et al. (2014), Widespread decline of Congo rainforest greenness in the past decade, *Nature*, *509*(7498), 86–90, doi:10.1038/nature13265.

Zhu, Z., J. Bi, Y. Pan, S. Ganguly, A. Anav, L. Xu, A. Samanta, S. Piao, R. R. Nemani, and R. B. Myneni (2013), Global data sets of vegetation leaf area index (LAI) 3g and fraction of photosynthetically active radiation (FPAR) 3g derived from Global Inventory Modeling and Mapping Studies (GIMMS) Normalized Difference Vegetation Index (NDVI3g) for the period 1981 to 2011, *Remote Sens. (Basel)*, *5*(2), 927–948.